TOPOLOGICAL CHARGES AND FLUX TUBES IN LATTICE QCD*

Š. OLEJNÍK†

Institute of Physics, Slovak Academy of Sciences
Bratislava, Slovakia
and
Institute for Nuclear Physics, Technical University
Vienna, Austria

(Received September 30, 1994)

The evidence for flux tubes from lattice QCD simulations is briefly reviewed. Then I present results of a detailed study of topological properties of QCD vacuum configurations below and above the deconfinement phase transition, both without and with dynamical quarks. The topological properties were probed by two local operators of topological-charge density and the cooling method. Results obtained using both definitions are compared and lessons from cooling experiments are briefly summarized. The flux-tube formation is seen to be reflected in topological-charge distributions.

PACS numbers: 12.38. Aw, 12.38. Gc

1. Introduction

Most phenomenological models (see *e.g.* [1–3]) describing strong interactions of quarks, antiquarks and gluons are based on a set of assumptions and postulates which are to a larger or lesser extent justified within the fundamental theory of quantum chromodynamics (QCD):

1. Quarks, antiquarks and gluons are confined, not observable (under normal conditions) as free particles in nature.

2. The vacuum is a non-trivial superposition of quark and gluon fields, which is not amenable to perturbative field-theory methods.

---

* Presented at the XXXIV Cracow School of Theoretical Physics, Zakopane, Poland, June 1–10, 1994.

† E-mail address: fyziolej@savba.savba.sk.

3. The quark and antiquark immersed in the vacuum are connected by a flux tube whose energy is proportional to its length. The medium inside the tube is essentially trivial, "perturbative".

4. Hadrons are "bags" of perturbative medium around their constituents, stabilized by the pressure of non-perturbative outside medium.

5. At high enough temperature (or higher density) a phase transition occurs, the transition from the phase of hadronic matter to that of free quarks and gluons (quark-gluon plasma). Flux tubes disappear above the deconfinement phase transition.

The lattice formulation of QCD and its Monte Carlo simulations (for an introduction and overview see [4]) are powerful tools for non-perturbative investigations of QCD predictions. In principle one should be able to compute any quantity to arbitrary precision like in quantum electrodynamics; in practice the precision is still limited by the power of existing computers and cleverness of algorithms used.

On the other hand, lattice is also useful in attempts to understand physical mechanisms of various strong-interaction phenomena like colour confinement (see *e.g.* Di Giacomo's lecture in Zakopane last year [5]) or chiral-symmetry breaking. An advantage of this branch of lattice QCD is the fact that a lot of qualitative information can be obtained even with moderate computers, working on smaller lattices and/or simulating a simplified version of QCD (quenched QCD, QCD with 2 colours) or even some lower-dimensional model.

Results that will be discussed in the present paper belong to the qualitative branch of lattice QCD. I will first briefly review various pieces of evidence that lattice QCD has provided to support the above-mentioned ingredients of phenomenological models, in particular about the properties of flux tubes (Section 2). Then I will present results of a recent investigation of topological properties of the QCD vacuum in the presence of static colour sources. First in Section 3 I discuss problems with the definition of topological charge on a lattice and describe a way how the problem is circumvented using the cooling method (for a thorough discussion see [6]). Lessons from our experiments with different variants of cooling are briefly summarized. Finally in Section 4 I present a sample of results of two runs for pure SU(3) lattice gauge theory, one at the temperature below and one above the deconfinement phase transition (Section 4.1.), and preliminary results of the third run, simulating full QCD with three quark flavours in the confinement phase (Section 4.2.). I will put particular emphasis on that part of our data that brings evidence for flux-tube formation and information on some properties of flux tubes. This work was done in collaboration with Faber, Markum and Sakuler from the Technical University in Vienna [7]. Section 5 contains a few concluding remarks.

2. Flux tubes in lattice QCD

The above-described flux-tube picture has been thoroughly tested in numerous lattice simulations. An indirect evidence was already contained in the earliest investigations [8]: the observed area-law behaviour of the Wilson loop of the size $R \times T$ ($R, T \gg a$, a is the lattice spacing)

$$W(R,T) \sim \exp(-\sigma A), \quad A = RT, \tag{1}$$

implies that the interaction potential $V(r)$ between an (infinitely) heavy quark and antiquark grows linearly with distance

$$V(r) \sim \sigma r \qquad \text{for} \quad r \to \infty, \tag{2}$$

which in turn can be most easily explained by a tube of constant energy density per unit length connecting the Q and $\bar{Q}$.

One can investigate flux tubes more directly by looking at various components of the colour electric and colour magnetic fields around a static $Q\bar{Q}$ pair. This is done by measuring correlations between the Wilson loop (or a pair of Polyakov lines) with plaquettes of different orientations. One can either use "disconnected" correlators [9]

$$\rho_W^{\text{disc}} = \frac{\langle \operatorname{Tr} W \operatorname{Tr} U_{\mu\nu} \rangle}{\langle \operatorname{Tr} W \rangle} - \langle \operatorname{Tr} U_{\mu\nu} \rangle, \tag{3}$$

or "connected" ones [10]

$$\rho_W^{\text{conn}} = \frac{\langle \operatorname{Tr}(W S U_{\mu\nu} S^\dagger) \rangle}{\langle \operatorname{Tr} W \rangle} - \frac{1}{2} \frac{\langle \operatorname{Tr} W \operatorname{Tr} U_{\mu\nu} \rangle}{\langle \operatorname{Tr} W \rangle} \tag{4}$$

(and analogous quantities with Polyakov lines). Here S denotes the Schwinger line connecting the Wilson loop W with the plaquette $U_{\mu\nu}$. In the formal continuum limit the former correlators behave as $a^4(\langle \operatorname{Tr} F_{\mu\nu}^2 \rangle_{Q\bar{Q}} - \langle \operatorname{Tr} F_{\mu\nu}^2 \rangle_0)$, while the latter should give $a^2(\langle \operatorname{Tr} F_{\mu\nu} \rangle_{Q\bar{Q}} - \langle \operatorname{Tr} F_{\mu\nu} \rangle_0)$, where $\langle \cdots \rangle_{Q\bar{Q}}$ denotes the average in the presence of a static $Q\bar{Q}$ pair and $\langle \cdots \rangle_0$ that in the vacuum. Obviously, the latter quantities are much easier to measure on a lattice, especially using the cooling method (the discussion of which will be postponed until Section 3).

The correlators (3) and (4) were measured in numerous lattice simulations [9–12] (the most recent high-statistics study is being performed by the Wuppertal group [13]). The results can be summarized as follows:

1. The dominant colour field component in the tube is the parallel (to the line joining Q and $\bar{Q}$) electric field, which is approximately constant along the tube.

2. All other field components are small.

3. The parallel electric field as a function of the transverse distance decreases exponentially; however, the exact dependence $E_{\parallel} = f(x_{\perp})$ has not been singled out by lattice data. A recent paper [14] shows that both

$$E_{\parallel} \sim \exp(-\mu^2 x_{\perp}^2) \tag{5}$$

and

$$E_{\parallel} \sim \left[1 + \mu x_{\perp} - \tfrac{1}{6}(\mu x_{\perp})^2\right] \exp(-\mu x_{\perp}), \tag{6}$$

give comparably good fits to measured data points.

4. Flux tubes become broader as $T \to T_c$.

5. In a simulation of full QCD with dynamical quarks an indication of flux-tube breaking due to light $q\bar{q}$ pair creation was observed [12].

Summarizing, the existence of flux tubes and their basic properties have been firmly established from first principles within lattice QCD. Here we will argue that information on flux tubes can also be obtained by studying topological characteristics of lattice configurations. Before doing that we have to briefly touch problems that arise in attempts to calculate topological quantities on a lattice.

3. Topological charges in lattice QCD

3.1. Definitions and problems

There exist in the literature various proposals of gauge-field configurations which could play an important role in the QCD vacuum [15, 16]. A basic observation for the classification of those configurations is the nontrivial topology of mappings from the surface of a sphere (in infinity) on the gauge group. According to the asymptotic behaviour of field configurations at infinity, they thus split into different classes, characterized by the *integer* winding number of the mapping (called often the topological charge, or Pontryagin index in mathematical language). There exist continuous transitions between configurations of the same class, but no continuous transitions between classes with different topological charges.

The topological charge Q is defined as an integral over the whole spacetime of the topological-charge density $q(x)$:

$$Q = \int d^4x q(x), \qquad q(x) = \frac{g^2}{64\pi^2} \epsilon^{\mu\nu\rho\sigma} F^a_{\mu\nu}(x) F^a_{\rho\sigma}(x). \tag{7}$$

Another important characteristic of the QCD vacuum is the topological susceptibility

$$\chi = \int d^4x \langle 0 \mid T(Q(x)Q(0)) \mid 0 \rangle, \tag{8}$$

which was proposed to solve the so-called U(1) problem [16, 17]. It is related to experimental quantities via the Witten–Veneziano formula [17]

$$\frac{2N_f}{f_\pi^2}\chi = m_\eta^2 + m_{\eta'}^2 - 2m_K^2\,, \tag{9}$$

(N_f is the number of light quark flavours, f_π the pion decay constant, m_η, $m_{\eta'}$ and m_K are masses of η-, η'- and K-mesons).

There is no unambiguous definition of the topological charge on a lattice (see *e.g.* [6]). Motivated by the aim to investigate the distribution of topological quantities *locally* around static quarks and antiquarks, we have chosen the definition of the topological charge through some local operator of topological-charge density $q_{\mathrm{L}}(x)$:

$$Q_{\mathrm{L}} = \sum_{\mathrm{sites}\,x} q_{\mathrm{L}}(x)\,; \qquad \chi_{\mathrm{L}} = \frac{\langle\, Q_{\mathrm{L}}^2 \,\rangle}{V}\,. \tag{10}$$

Even this choice is not unique, since various operators converge in the formal continuum limit to the continuum topological-charge density. We used two common definitions:

$$q_{\mathrm{L}}^{(P)}(x) = -\frac{1}{2^4 32\pi^2} \sum_{\mu\nu\rho\sigma=\pm1}^{\pm4} \tilde{\epsilon}_{\mu\nu\rho\sigma}$$
$$\times \mathrm{Tr}[U_\mu(x)U_\nu(x+\mu)U_\mu^\dagger(x+\nu)U_\nu^\dagger(x)U_\rho(x)U_\sigma(x+\rho)U_\rho^\dagger(x+\sigma)U_\sigma^\dagger(x)] \tag{11}$$

("plaquette" definition [18, 19]), and

$$q_{\mathrm{L}}^{(H)}(x) = -\frac{1}{2^4 32\pi^2} \sum_{\mu\nu\rho\sigma=\pm1}^{\pm4} \tilde{\epsilon}_{\mu\nu\rho\sigma}\, \mathrm{Tr}[U_\mu(x)U_\nu(x+\mu)U_\rho(x+\mu+\nu)$$
$$\times U_\sigma(x+\mu+\nu+\rho)U_\mu^\dagger(x+\nu+\rho+\sigma)U_\nu^\dagger(x+\rho+\sigma)U_\rho^\dagger(x+\sigma)U_\sigma^\dagger(x)] \tag{12}$$

("hypercube" definition, proposed by Di Vecchia *et al.* [18]).[1]

With both above choices one immediately runs into troubles: at finite coupling constant β ($= 6/g^2$) and finite lattice spacing a

[1] More precisely, we use a slightly different definition of the density than the one given in Eq. (12). In this definition all 16 vertices of a hypercube are treated symmetrically and the density is not attributed to the sites of the lattice, but to those of the dual lattice. For details see the papers of Di Vecchia *et al.* [18].

1. measured topological charges are *not integer*, and
2. the topological susceptibility is *too small* compared to the value expected on the basis of Eq. (9).

These difficulties of the method were known for years and were not considered surprising. In early years of lattice-gauge-theory calculations many authors believed that attempts to calculate χ on the lattice were doomed to failure, since the topological properties of the continuum are different from those of discretized space-time.

The real origin of both problems has been explained by Campostrini *et al.* [20]: lattice and continuum versions of the theory represent different renormalized quantum field theories, which differ from one another by finite, non-negligible renormalization factors:

$$q_{\mathrm{L}}(x) = a^4 Z(\beta) q(x) + O(a^6)\,, \tag{13}$$

$$\chi_{\mathrm{L}} = a^4\, Z^2(\beta)\, \chi + a^4\, M_G(\beta)\, G_2 + a^4\, M_\psi\, \langle m\, \bar{\psi}\psi \rangle + P(\beta)\, \langle \mathbf{1} \rangle + O(a^6)\,. \tag{14}$$

The multiplicative renormalization constant $Z(\beta)$ approaches 1 for $\beta \to \infty$, but is rather small for values of β used in numerical simulations [20, 21]. For SU(3) and the above operators of $q_{\mathrm{L}}(x)$ one has:

$$Z^{(P)} \simeq 1 - \frac{5.4508}{\beta} + \frac{11.0766}{\beta^2}\,, \tag{15}$$

$$Z^{(H)} \simeq 1 - \frac{6.1296}{\beta} + \frac{11.2310}{\beta^2}\,, \tag{16}$$

in two-loop approximation. The functions $P(\beta)$, $M_G(\beta)$, $M_\psi(\beta)$ can also be calculated perturbatively as power series in β^{-1}; the first few terms are known analytically, the others can (in principle) be estimated numerically (see [22]).

3.2. Cooling

If one wants to make use of the above definition of the topological charge, Eqs (10)–(12), one must either carefully take into account the renormalization factors $Z(\beta)$, *etc.*, or to use some procedure to eliminate them. Fortunately such a procedure exists and is called the method of *cooling* [23–25]. It is a way of "smoothening" field configurations and at the same time removing ultraviolet quantum fluctuations. Practically, the cooling procedure consists of replacing each link of a configuration by a new link which locally minimizes the action. A cooling step is defined as sequential cooling of all links of the configuration. If changes of the links are kept sufficiently small, each cooling step can be considered as the lattice version

of a smooth deformation of a continuum field configuration to a new one with smaller action, which reduces quantum fluctuations, but preserves the topology of the initial configuration. Thus cooling brings us to the minimum action configuration of the topological sector to which the initial configuration belonged. However, since classical solutions of the continuum equations of motion correspond only to approximate solutions on a lattice, they will be only metastable. The probability of immediate transitions to different topological sectors can be reduced by controlling the speed of cooling.

There exist various variants of cooling. We have implemented and tested three different procedures:

1. *mild "Metropolis" cooling* [24, 25]: in this procedure all links of the configuration are updated using the usual Metropolis update procedure (with a small spread of changes of the link matrices), but changes are only accepted if the action is decreased and the changes are rather small [25], namely

$$\tfrac{1}{3}\,\mathrm{Tr}\left\{(U_\mu^\dagger - U_\mu'^\dagger)(U_\mu - U_\mu')\right\} \leq \delta^2\,; \tag{17}$$

2. *smearing* [26, 27][2]: here links are transformed to

$$U_\mu' = \Pi\left[U_\mu + \epsilon \sum_{\eta=-1,1} \sum_{\nu\neq\mu} S_{\mu\nu}^\eta\right], \tag{18}$$

where $S_{\mu\nu}^\eta$ is the staple (incomplete plaquette) with orientation η in direction ν for the link μ, and $\Pi[A]$ stands for the projection of a matrix A onto the SU(3) manifold;

3. *"Cabibbo–Marinari" cooling* [24]: this is analogous to the Cabibbo–Marinari [28] heat-bath algorithm, which updates the SU(3) link variable by updating some of its SU(2) subgroups. A cooling step in this method consists of multiplying the link variable with a matrix V from a diagonal SU(2) subgroup,

$$U_\mu(x) \to V U_\mu(x)\,, \tag{19}$$

where V is chosen in such a way that within this class of transformations the action is locally minimized[3]. Within a cooling step, we minimize in all three diagonal subgroups, in random order. We also check after each minimization step that the condition (17) is fulfilled.

---

[2] Strictly speaking, smearing is not a cooling procedure, however, the behaviour of lattice configurations under smearing is very similar to cooling.

[3] This matrix can be found analytically and the calculation is approximately as time-consuming as a normal Metropolis sweep.

We performed a series of experiments to reveal similarities and differences among these three cooling/smearing variants (more details can be found in [29]). Summarizing the results in brief, we should stress the following points:

1. *Independence of observed effects on the cooling variant.* With suitably chosen parameters δ and ϵ, Eqs (17), (18), the observed physical effects did not depend strongly on the cooling method. In most tests $\delta = 0.15$ and $\epsilon = 0.1$ were used, but rather substantial changes of both parameters changed the cooling process only slightly. *E.g.* in the Cabibbo–Marinari variant even an order of magnitude decrease of δ influenced only the first few cooling steps. Similarly, in this variant it was rather unessential whether one minimized in three diagonal SU(2) subgroups in a random manner or in some ordered one (*e.g.* 1–2–3).

2. *Different efficiency of cooling variants.* The speed of cooling, on the other hand, was a distinctive feature of the three methods. With the Cabibbo–Marinari cooling all measured configurations reached (close to) integer values of topological charge quite quickly, in 5–10 steps, in both other variants almost 100 cooling steps were mostly needed. The typical behaviour of Q under cooling and smearing is shown in figure 1, for two configurations with $Q = \pm 1$. The efficiency of the Cabibbo–Marinari cooling was the main reason why we used this particular variant in all our production runs (see below).

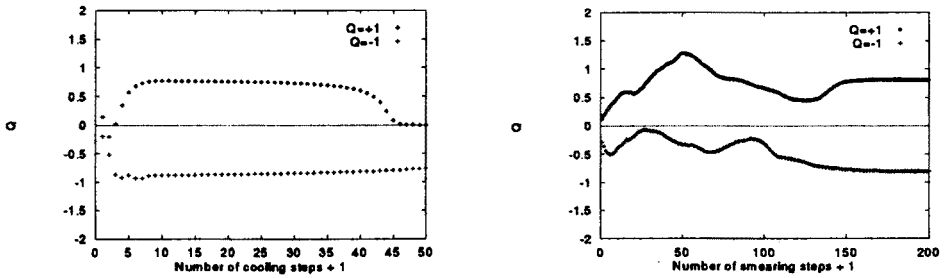

(a) (b)

Fig. 1. Behaviour of the topological charge of two thermalized pure SU(3) configurations at $\beta = 5.6$ under cooling/smearing (topological charge was obtained using the plaquette definition of charge density): (a) Cabibbo–Marinari cooling with $\delta = 0.15$, (b) smearing with $\epsilon = 0.1$.

3. *Relative stability of cooling.* The cooling process was essentially independent of the start configuration. This fact is nicely illustrated in figure 2, where the energies of configurations are shown after 0–5 cooling steps, for both our pure gauge simulations. The energies decrease with cooling, but for a given cooling step cluster around well-defined average values.

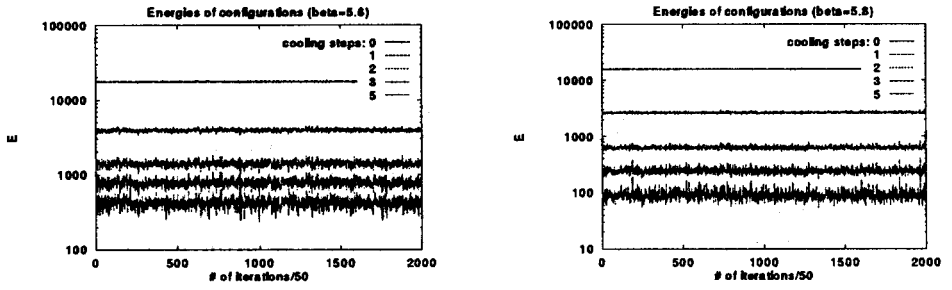

(a) (b)

Fig. 2. Energies of individual pure-gauge configurations at $\beta = 5.6$ (a) and 5.8 (b) after 0–3 and 5 cooling steps. (Scales are different in both figures.)

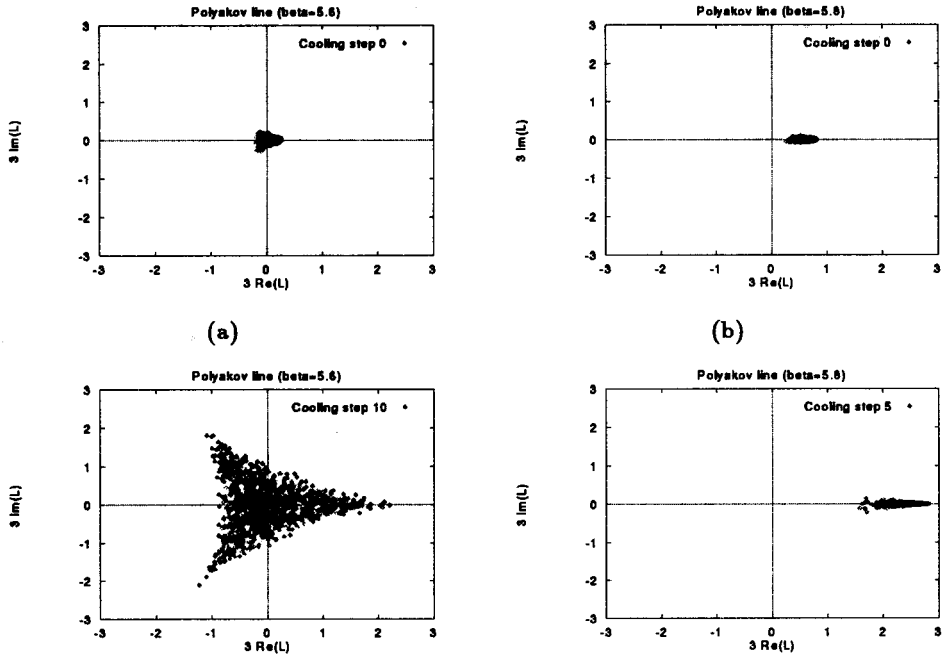

(a) (b)

(c) (d)

Fig. 3. Real vs. imaginary parts of average Polyakov lines for measured pure-gauge configurations.

4. *Cooling does not destroy confinement,* at least during first $O(10)$ steps of the Cabibbo–Marinari cooling. An order parameter of confinement for pure gauge theory is the average value of the real part of the Polyakov loop

$$L(\vec{r}) = \tfrac{1}{3}\,\mathrm{Tr}\prod_{t=1}^{N_t} U_4(\vec{r},t)\,. \tag{20}$$

In the confinement phase this value was always consistent with 0 within errors during cooling, while in the deconfinement phase it was non-zero and grew with the number of cooling steps to 1. Thus cooling not only preserves the (de)confining character of configurations, but in fact makes differences between both phases more visible. This is illustrated in figure 3. The "Mercedes-star" plot typical for the confinement phase of pure gauge theory with unbroken Z_3 symmetry is clearly seen already after 5–10 cooling steps; in the deconfinement phase the Z_3 symmetry is broken and only one corner of the "star" is occupied.

5. *Cooling indeed removes renormalization factors.* Before cooling topological charges measured using the plaquette or hypercube definition were different and rather small. The difference between $Q^{(P)}$ and $Q^{(H)}$ is caused by different renormalization factors $Z^{(P)}(\beta)$ and $Z^{(H)}(\beta)$, Eqs (15), (16). It disappears after the first few cooling steps, see figure 4. Also, after $O(10)$ cooling steps all charges group around values (approximately) given by $Q = n\,Q_1$, with $n = 0, \pm 1, \ldots$, and the "unit" charge Q_1 slightly smaller than 1 (this number depends on β and the lattice size [30]).

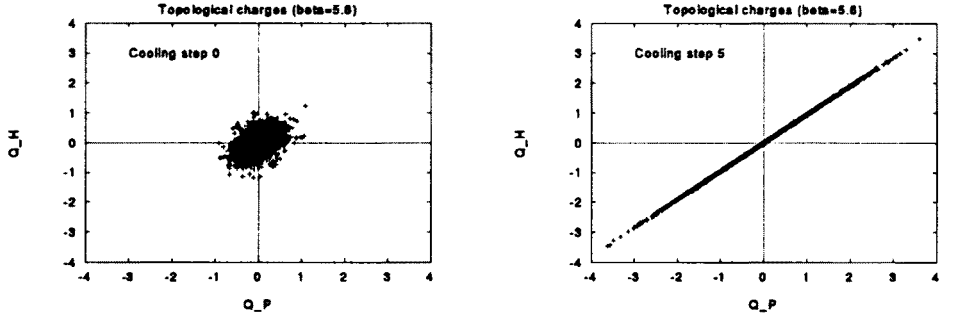

(a) (b)

Fig. 4. $Q^{(P)}$ vs. $Q^{(H)}$ at $\beta = 5.6$: (a) before cooling, (b) after 5 cooling steps.

4. Flux tubes in topological-charge distributions

Finally I come to the central part of my lecture. I will present (a subset of) our results on topological contents of lattice gauge-field configurations in both the confinement and deconfinement phase. We performed three runs, simulating QCD with 3 colours, on an $8^3 \times 4$ lattice, with periodic boundary conditions. The parameters of the runs were:

- RUN 1: without dynamical quarks, with standard Wilson action, $\beta = 5.6$ (*confinement phase*);

- RUN 2: without dynamical quarks, with standard Wilson action, $\beta = 5.8$ (*deconfinement phase*);
- RUN 3: with 3 flavours of (Kogut–Susskind) quarks, standard Wilson action for gauge fields, all three quark masses equal: $m_q a = 0.1$, $\beta = 5.2$ (again *confinement phase*).

In each run we made 100000 iterations and measured observables of interest after every 50th iteration. Each of this subsample of 2000 configurations was subjected to 50 cooling steps, using the "Cabibbo–Marinari" cooling method of Ref. [24]. In Section 4.1 I summarize results from pure-gauge simulations (RUN 1 and 2), Section 4.2 contains first results from our full-QCD run (RUN 3).

4.1. QCD without dynamical quarks

Our simulations were performed at two values of the coupling constant β, one corresponding to the confinement phase and the other to the deconfinement one.

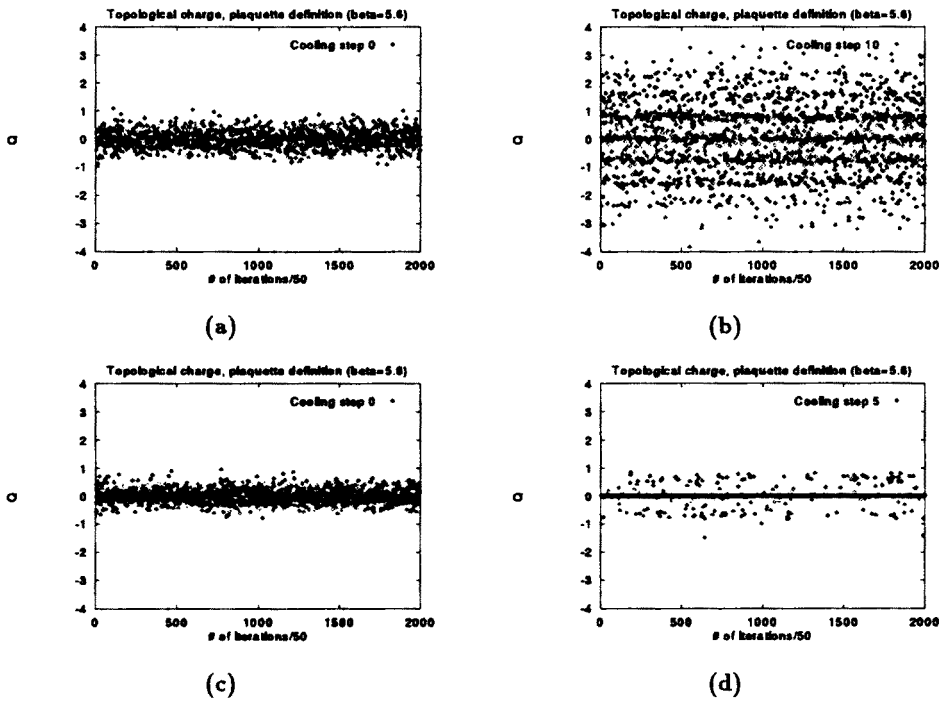

Fig. 5. Topological charges of measured pure-gauge configurations obtained using the "plaquette" definition of the topological-charge density.

We have already stated that cooling quickly removed differences between topological charges of lattice configurations measured using the plaquette or hypercube definition. I will therefore in most cases discuss results obtained using the former choice. Figure 5 shows how the originally small non-integer values of charges cluster around approximately integer values after 10 cooling steps at $\beta = 5.6$ and already after 5 cooling steps at $\beta = 5.8$. A least-square fit gives a value of the "unit" charge $Q_1 \simeq 0.8$ at $\beta = 5.6$ and $Q_1 \simeq 0.7$ at $\beta = 5.8$. The probability distributions of various integer values are shown in figure 6.

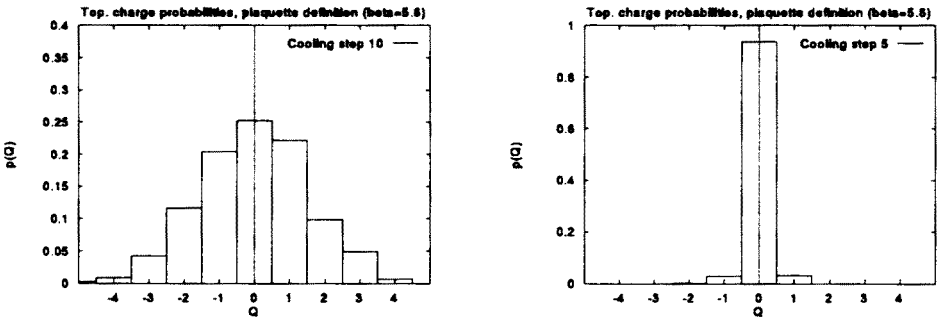

(a) (b)

Fig. 6. Probabilities for various values of the topological charge (in units of $Q_1 \simeq 0.8$ for $\beta = 5.6$, $Q_1 \simeq 0.7$ for $\beta = 5.8$).

From the above figures one can already deduce the first essential difference between the confinement and deconfinement configurations. In both phases the $Q = 0$ sector dominates, but in the confinement phase also higher charges are quite probable (in more than 70% of configurations), while in the deconfinement one $Q \neq 0$ appears only very rarely. Polikarpov and Veselov [31] suggested to plot $\ln\left[p(Q) \pm \sqrt{p(Q)}\right]$ as a function of Q^2. A linear dependence is a sign for a Gaussian distribution. Figure 7 plots our results after 10 cooling steps at $\beta = 5.6$: the data are clearly consistent with a linear decrease of $\ln\left[p(Q) \pm \sqrt{p(Q)}\right]$ with Q^2.

What now happens if a static quark or a static quark-antiquark pair is present? The time propagation of a static quark at finite temperature T $(= 1/N_t a)$ is described by the Polyakov loop $L(\vec{r})$, Eq. (20). To obtain the local distribution of the topological-charge density around single quarks and around a meson with quark-antiquark separation d we calculate the correlation functions

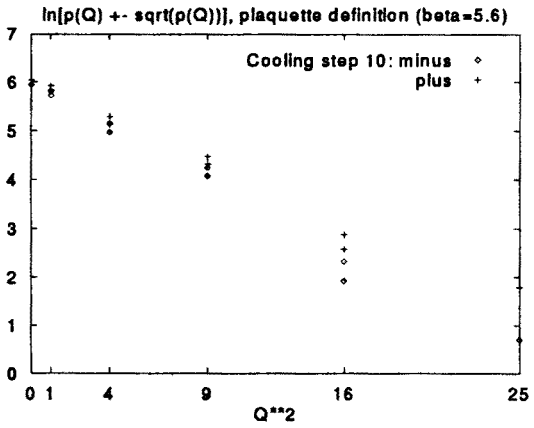

Fig. 7. $\ln[p(Q) \pm \sqrt{p(Q)}]$ vs. Q^2 after 10 cooling steps at $\beta = 5.6$. (Units on the vertical axis are arbitrary.)

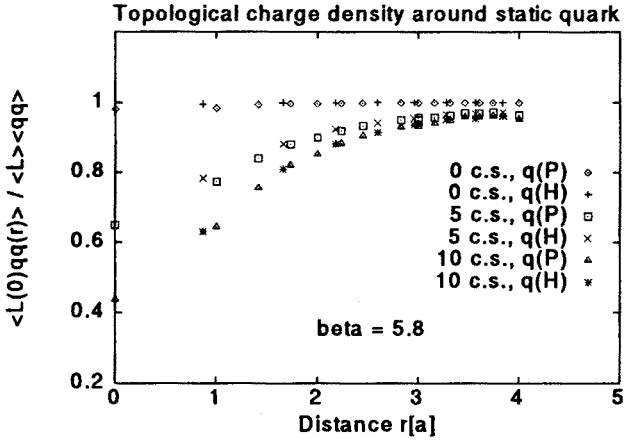

Fig. 8. Squared topological-charge density around a static quark after 0, 5, and 10 cooling steps at $\beta = 5.8$ (deconfinement phase).

$$\langle L(0)q^2(r)\rangle \tag{21}$$

and

$$\langle L(0)L^\dagger(d)q^2(r)\rangle\,, \tag{22}$$

respectively, and normalize them to the corresponding vacuum expectation values (if they are not equal to 0). We take the square of the topological-charge density in Eqs (21), (22), the simplest choice leading to nontrivial correlations.

In the confinement phase one expects $\langle L(0)q^2(r)\rangle = 0$, since a single quark is a forbidden state.[4] This expectation was confirmed by our measurements.

In figure 8 we show the square of the topological-charge density around a single static *quark* in the deconfinement phase after 0, 5, and 10 cooling steps, for both definitions of the density. *We see a suppression of the density close to the position of the quark source.* Results from both definitions of the density agree perfectly after a few cooling steps. The agreement is far from obvious, since the topological-charge densities in figure 8 were calculated at different distances for both definitions. This is due to the fact that the plaquette definition gives topological-charge density in a lattice site, while the hypercube one rather in the center of the hypercube (in a site of the dual lattice).

In figure 9 distributions of the topological-charge density (squared) around a *meson* are presented for both phases of pure SU(3), after 5 cooling

Topological-charge density in a static meson

$\beta = 5.6$ $\beta = 5.8$

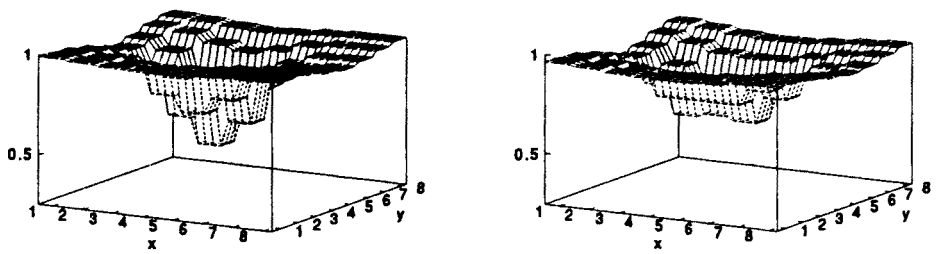

(a) 5 cooling steps, d = 2

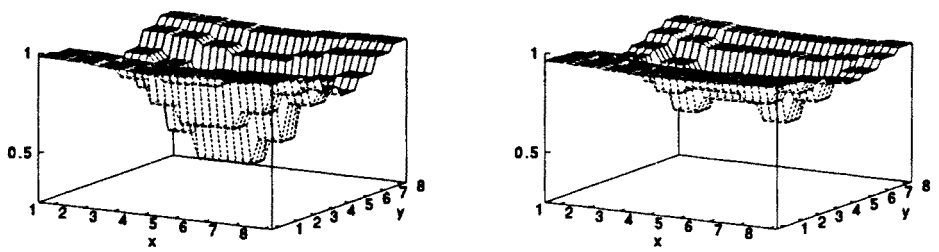

(b) 5 cooling steps, d = 3

[4] More formally one can argue that the operator of topological-charge density is Z_3 symmetric, while the Polyakov loop is not. Since Z_3 symmetry is unbroken in the confinement phase, the average $\langle L(0)q^2(r)\rangle$ must be zero.

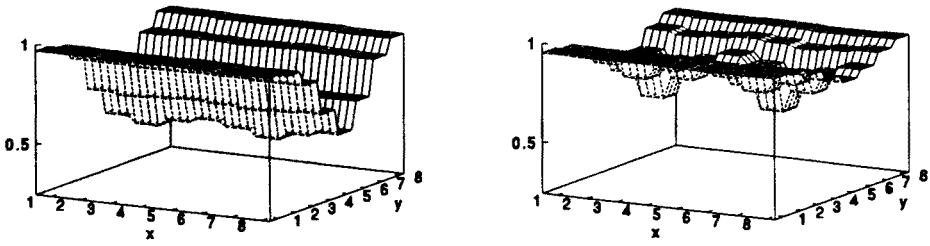

(c) 5 cooling steps, d = 4

Fig. 9. Squared topological-charge density around a static quark-antiquark pair at $\beta = 5.6$ and $\beta = 5.8$.

steps at distances $d = 2$, 3 and 4. The suppression in the vicinity of sources is again clearly visible, the effect is stronger in the confinement regime. The difference between both phases is most striking at the largest separation, $d = 4$. The valley of suppressed topological-charge density in the confinement phase reflects the formation of a flux tube between the static quark-antiquark pair. In the deconfinement phase, no flux tube is visible.

4.2. QCD with dynamical quarks

It is expected that qualitative features of colour confinement are the same in QCD without and with dynamical quarks. However, the effect of dynamical quarks has to be taken into account in any realistic calculation. The account of dynamical quarks and non-zero quark masses is also important for understanding the connection to other physical phenomena like chiral-symmetry breaking.

The topological susceptibility is one of the quantities for which the introduction of quarks plays a vital role. In a theory with fermions one expects the topological susceptibility to be proportional to (a power of) the quark mass, namely [32]

$$\chi \sim \frac{m_q}{n_f^2}\langle\bar{\psi}\psi\rangle\,, \tag{23}$$

in the chirally broken (confinement) phase, while

$$\chi \sim m_q^{n_f}\,, \tag{24}$$

in the chirally symmetric deconfinement phase (n_f is the number of light flavours of quarks with mass m_q). Therefore one can reasonably expect that though the effects due to topology may be qualitatively similar in full QCD to pure-gauge QCD, the magnitude of observed effects will depend on the presence of dynamical quarks and their masses.

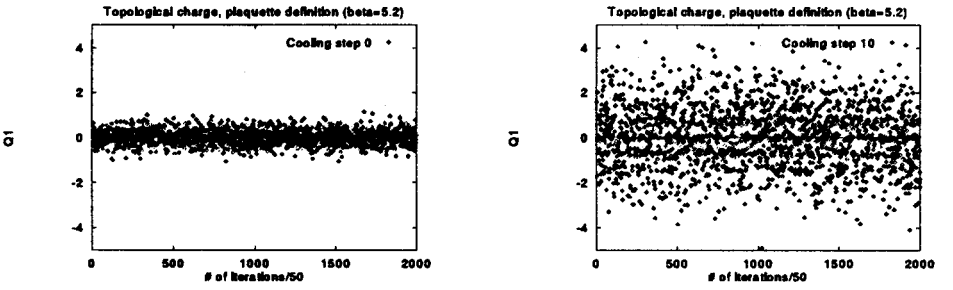

(a) (b)

Fig. 10. Topological charges of measured configurations in the run with dynamical quarks.

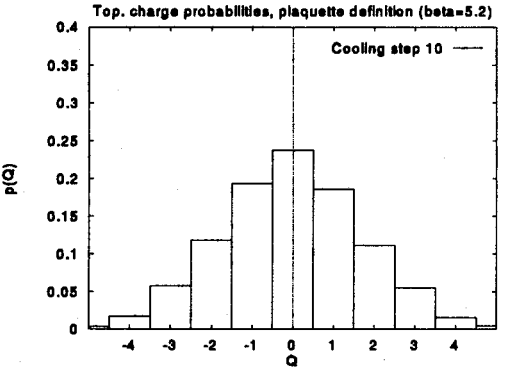

Fig. 11. Probabilities for various values of the topological charge at $\beta = 5.2$.

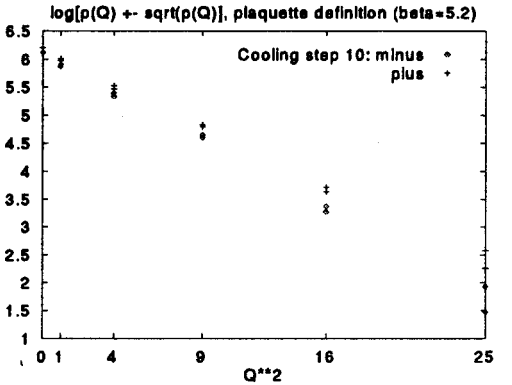

Fig. 12. $\ln[p(Q) \pm \sqrt{p(Q)}]$ vs. Q^2 after 10 cooling steps at $\beta = 5.2$. (Units on the vertical axis are arbitrary.)

Topological-charge density in a static meson

$\beta = 5.2, n_f = 3, m_q a = 0.1$

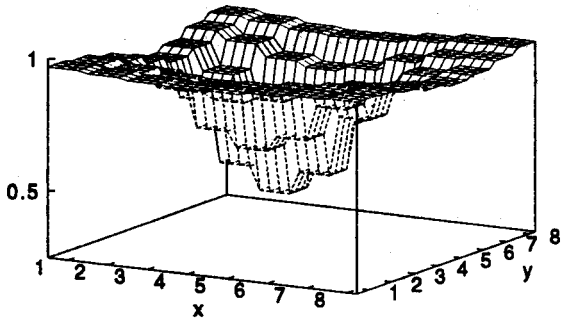

(a) 5 cooling steps, d = 2

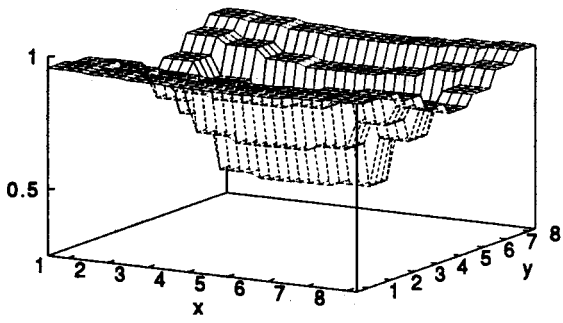

(b) 5 cooling steps, d = 3

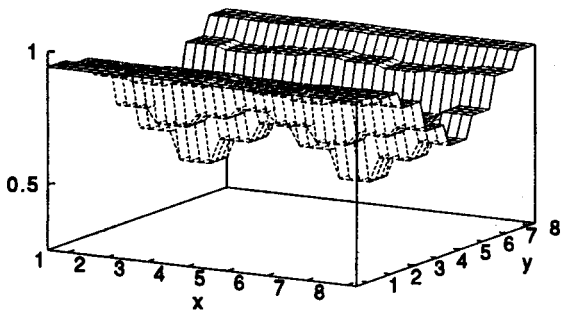

(c) 5 cooling steps, d = 4

Fig. 13. Squared topological-charge density around a static quark-antiquark pair at $\beta = 5.2$.

The parameters of our RUN 3 with dynamical fermions were chosen in such a way so that we could compare results with that of our RUN 1. The *physical* length scale of the lattice is similar in both simulations, and both correspond to the confinement phase.

The results are indeed very similar. The reader should *e.g.* compare figure 5(a), 5(b) with figure 10 or figure 6(a) with figure 11. The probability distribution of various topological-charge values is again Gaussian, though somewhat broader (figure 12).

The essential difference between pure SU(3) results and those from simulations including dynamical fermions is comprised in figure 13. Again a suppression of topological-charge density occurs in the whole flux tube between the quark and antiquark, but the situation changes at the largest separation, $d = 4$. In the middle of the tube the suppression is weaker than in the pure-gauge case. This we consider an indication of flux-tube breaking due to a creation of a virtual (dynamical) $q\bar{q}$ pair. A similar effect was observed earlier also in colour field distributions around a static quark-antiquark system, see [12].

Though our results from the first run with dynamical fermions are promising, a word of caution is necessary. Our value of the quark mass is still rather high and not realistic. The mass dependence of the observed effects would be of immediate interest. We plan to study this problem in a near future.

5. Concluding remarks

The flux-tube picture has undergone a series of tests in lattice QCD. With present-day lattice techniques and computer power one is already able to observe flux-tube formation over distances as large as 2 fm [13]. One of the important pieces of strong-interaction models thus becomes fully established from first principles of QCD.

Results of our work, obtained on a rather small lattice with a modest computer, cannot bring more than qualitative support for phenomenological models. That is also the reason why our data can hardly be used to discriminate between various models.

Nevertheless, we find quite interesting that the existence of flux tubes reflects itself not only on physical quantities like the energy or action density. We have demonstrated that even the topological observables "feel" the flux tube connecting the static quark and antiquark. This is another confirmation of the idea that the media "inside" and "outside" the tube are different and differ even in their topological properties.

To identify gauge-field configurations that determine properties of the QCD vacuum and drive the flux-tube formation in the confinement phase

of QCD remains a challenging task, both in the continuum and the lattice version of the theory.

I would like to thank the organizers of the School for invitation and hospitality in Zakopane. I am also grateful to M. Faber, H. Markum and W. Sakuler for many discussions and collaboration. This work was supported by Bundesministerium für Wissenschaft und Forschung (Austria) and by the Slovak Grant Agency for Science, Contract No. 2/1157/94.

REFERENCES

[1] R.F. Alvarez-Estrada, F. Fernandez, J.L. Sánchez-Gomez, V. Vento, *Models of Hadron Structure Based on QCD*, Springer, Berlin 1986.

[2] E.V. Shuryak, *The QCD Vacuum, Hadrons and the Superdense Matter*, World Scientific, Singapore 1988.

[3] A. Chodos, R.L. Jaffe, K. Johnson, C.B. Thorn, V. Weisskopf, *Phys. Rev.* **D9**, 3471 (1974).

[4] R. Gupta, *Acta Phys. Pol.* **B26**, No 1 (1995) in press; H.J. Rothe, *Lattice Gauge Theories. An Introduction*, World Scientific, Singapore 1992.

[5] A. Di Giacomo, *Acta Phys. Pol.* **B25**, 215 (1994).

[6] A. Di Giacomo, *Acta Phys. Pol.* **B25**, 227 (1994).

[7] M. Faber, H. Markum, Š. Olejník, W. Sakuler, *Phys. Lett.* **B334**, 145 (1994); *Nucl. Phys.* **B34** (Proc. Suppl.), 167 (1994) and a paper in preparation.

[8] M. Creutz, *Phys. Rev. Lett.* **43**, 553 (1979); *Phys. Rev. Lett.* **45**, 313 (1980); *Phys. Rev.* **D21**, 2308 (1980).

[9] M. Fukugita, T. Niuya, *Phys. Lett.* **B132**, 374 (1983).

[10] A. Di Giacomo, M. Maggiore, Š. Olejník, *Phys. Lett.* **B236**, 199 (1990); *Nucl. Phys.* **B347**, 441 (1990); M. Campostrini, A. Di Giacomo, M. Maggiore, Š. Olejník, H. Panagopoulos, E. Vicari, *Nucl. Phys.* **B** (Proc. Suppl.) **17**, 563 (1990).

[11] J. Flower, S. Otto, *Phys. Lett.* **B160**, 128 (1985); J. Wosiek, R. Haymaker, *Phys. Rev.* **D36**, 3297 (1987); R. Sommer, *Nucl. Phys.* **B291**, 673 (1987); *Nucl. Phys.* **B306**, 180 (1988); D.G. Caldi, T. Sterling, *Phys. Rev. Lett.* **60**, 2454 (1988); R.W. Haymaker, J. Wosiek, *Phys. Rev.* **D43**, 1991 (1990); *Acta Phys. Pol.* **B21**, 403 (1990); R.W. Haymaker, Y. Peng, V. Singh, J. Wosiek, *Nucl. Phys.* **B** (Proc. Suppl.) **17**, 558 (1990); R.W. Haymaker, V. Singh, J. Wosiek, *Nucl. Phys.* **B** (Proc. Suppl.) **20**, 207 (1991); T. Barczyk, R.W. Haymaker, V. Singh, E. Laermann, J. Wosiek, *Nucl. Phys.* **B** (Proc. Suppl.) **26**, 462 (1992); Y. Peng, R.W. Haymaker, *Phys. Rev.* **D47**, 5104 (1993); T. Barczyk, *Nucl. Phys.* **B** (Proc. Suppl.) **30**, 499 (1993).

[12] W. Feilmair, H. Markum, *Nucl. Phys.* **B370**, 299 (1992).

[13] G.S. Bali, K. Schilling, Ch. Schlichter, *Nucl. Phys.* **B** (Proc. Suppl.) **34**, 216 (1994); Observing Long Colour Flux Tubes in SU(2) Lattice Gauge Theory, preprint CERN-TH.7413/94, WUB 94-24, hep-lat/9409005 (1994).

[14] L. Del Debbio, A. Di Giacomo, Yu.A. Simonov, *Phys. Lett.* **B332**, 111 (1994).
[15] A.A. Belavin, A.M. Polyakov, A.A. Schwartz, Yu.S. Tyupkin, *Phys. Lett.* **B59**, 85 (1975).
[16] G. 't Hooft, *Phys. Rev. Lett.* **37**, 8 (1976); *Phys. Scr.* **25**, 133 (1982).
[17] G. Veneziano, *Nucl. Phys.* **B159**, 213 (1979); E. Witten, *Nucl. Phys.* **B156**, 269 (1979).
[18] P. Di Vecchia, K. Fabricius, G. Rossi, G. Veneziano, *Nucl. Phys.* **B192**, 392 (1981); *Phys. Lett.* **B108**, 323 (1982).
[19] K. Ishikawa, G. Schierholz, H. Schneider, M. Teper, *Phys. Lett.* **B128**, 309 (1983); N.V. Makhaldiani, M. Müller-Preußker, *JETP Lett.* **37**, 523 (1983).
[20] M. Campostrini, A. Di Giacomo, H. Panagopoulos, *Phys. Lett.* **B212**, 206 (1988).
[21] B. Allés, A. Di Giacomo, M. Giannetti, *Phys. Lett.* **B249**, 490 (1990).
[22] B. Allés, M. Campostrini, A. Feo, H. Panagopoulos, *Nucl. Phys.* **B** (Proc. Suppl.) **30**, 243 (1993).
[23] B. Berg, *Phys. Lett.* **B104**, 475 (1981); E.M. Ilgenfritz, M.L. Laursen, M. Müller-Preußker, G. Schierholz, H. Schiller, *Nucl. Phys.* **B268**, 693 (1986).
[24] M. Teper, *Phys. Lett.* **B162**, 357 (1985); **B171** (1986) 81, 86; J. Hoek, M. Teper, J. Waterhouse, *Nucl. Phys.* **B288**, 589 (1987).
[25] M. Campostrini, A. Di Giacomo, H. Panagopoulos, E. Vicari, *Nucl. Phys.* **B329**, 683 (1990).
[26] APE Collaboration, M. Albanese *et al.*, *Phys. Lett.* **B192**, 163 (1987).
[27] M. Campostrini, A. Di Giacomo, Y. Gündüç, M.P. Lombardo, H. Panagopoulos, R. Tripiccione, *Phys. Lett.* **B252**, 436 (1990).
[28] N. Cabibbo, E. Marinari, *Phys. Lett.* **B119**, 387 (1982).
[29] W. Sakuler, Topologische Ladungsdichte um statische Quarks in der Gitter-Quantenchromodynamik, PhD thesis, Techn. Univ. Wien 1994.
[30] B. Allés, M. Campostrini, A. Di Giacomo, Y. Gündüç, E. Vicari, *Phys. Rev.* **D48**, 2284 (1993).
[31] M.I. Polikarpov, A.I. Veselov, *Nucl. Phys.* **B297**, 34 (1988).
[32] J.B. Kogut, D.K. Sinclair, M. Teper, *Nucl. Phys.* **B348**, 178 (1991).